Generation of identical photons using an electrically driven single-photon source

Raj B. Patel[a,b], Anthony J. Bennett[b], Ken Cooper[a], Paola Atkinson[a]*, Christine A. Nicoll[a], David A. Ritchie[a], and Andrew J. Shields[b]

[a]Cavendish Laboratory, Cambridge University, JJ Thomson Avenue, Cambridge, CB3 0HE, U. K.;

[b]Toshiba Research Europe Limited, Cambridge Research Laboratory, 208 Cambridge Science Park, Milton Road, Cambridge, CB4 0GZ, U. K.

ABSTRACT

A single-photon source capable of emitting indistinguishable photons is a key element in schemes for scalable quantum information processing with linear optics. Whilst several groups have reported such sources, up until now an electrically driven source capable of making these protocols technologically viable has yet to be reported. We present the first demonstration of an electrically driven single-photon source emitting indistinguishable photons. Our sample consists of a layer of InAs/GaAs quantum dots embedded in the intrinsic region of a p-i-n microcavity diode. We test the indistinguishability of consecutive photons by carrying out a Hong-Ou-Mandel-type two-photon interference experiment whereby two identical photons arriving simultaneously at two input ports of a 50:50 beamsplitter exit together. The device was operated under two modes, continuous and pulsed current injection. In the former case, we measured a coherence time of up to 400 ps at low pump current - the longest reported under these excitation conditions. A two-photon interference visibility was measured, limited only by the timing resolution of our detection system and further suggesting a 100% overlap of photon wavepackets at the output beamsplitter. In the case of pulsed injection, we employed a two-pulse voltage sequence which allowed us to carry out temporal filtering of photons which had undergone dephasing. The characteristic Hong-Ou-Mandel "dip" was measured resulting in a visibility of 64 ± 4%.

Keywords: Quantum dot, diode, single-photon source, photon statistics, Hong-Ou-Mandel, quantum interference, quantum information

1. INTRODUCTION

Quantum information science promises many advantages over classical information processing. While non-classical elements such as entanglement and quantum interference have been readily demonstrated using parametric down-conversion,[1,2] the proposal of scalable quantum information processing[3] has stimulated many efforts in finding suitable two-level systems which may act as single-photon sources. With the exception of quantum cryptography, these schemes place a strict requirement on single-photon sources in that the photons must be in a pure state such that consecutive photons are identical. The standard approach to testing the indistinguishability is by carrying out a Hong-Ou-Mandel[1] two-photon interference experiment where photons from the source are sent into the two inputs of a 50:50 beamsplitter. For photons that are indistinguishable in space, time, energy and polarization, the photon wavepackets overlap perfectly ($\langle\psi_1|\psi_2\rangle = 1$) resulting in a bunching behavior as illustrated in Figure 1. Experimentally this can observed as a suppression in coincident counts at two detectors placed in the output ports the beamsplitter.

Several groups have demonstrated the emission of indistinguishable photons from single-photon sources such as molecules,[4] atoms,[5] ions,[6] and semiconductor quantum dots.[7] Quantum dots are of particular interest as they can be grown to suit a particular application and can undergo fluorescence with either optical excitation or

*Now at: Max-Planck-Institut für Festkörperforschung, Heisenbergstr.1, D-70569 Stuttgart, Germany.
Further author information: Send correspondence to R.B.P.: E-mail: rp349@cam.ac.uk or A.J.B.: E-mail: anthony.bennett@crl.toshiba.co.uk

Quantum Dots, Particles, and Nanoclusters VI,
edited by Kurt G. Eyink, Frank Szmulowicz, Diana L. Huffaker, Proc. of SPIE Vol. 7224,
72240X · © 2009 SPIE · CCC code: 0277-786X/09/$18 · doi: 10.1117/12.808150

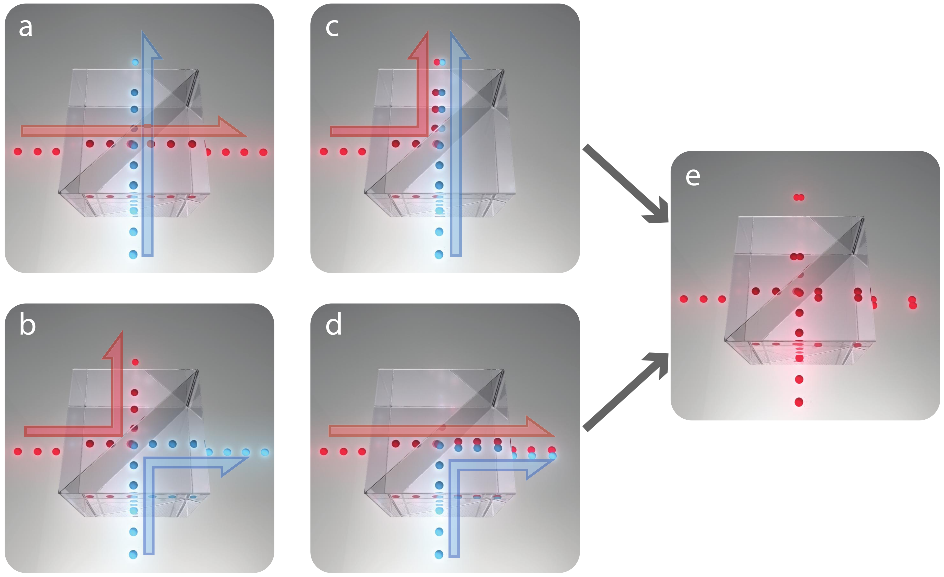

Figure 1. Hong-Ou-Mandel interference at a 50:50 beamsplitter. (a)-(d) show the four possible paths the photons can take. If the photons are identical, the two-photon probability amplitudes in (a) and (b) cancel resulting in the bunching behaviour shown in (e).

electrical injection. Since a quantum dot is not an isolated system, phononic[8–11] and Coulombic[12,13] interactions with the exciton complex can lead to dephasing. This is especially true under non-resonant electrical injection.[14] Jitter in the photon emission time and dephasing can both contribute to a reduction in the measured two-photon interference visibility. Visibility can be restored by using a high-Q, low modal volume cavity to reduce the radiative lifetime T_1 to the point where the coherence time T_2 is limited only by the length of the photon wavepacket.[7] From the optical Bloch equations, these times are related by

$$\frac{1}{T_2} = \frac{1}{2T_1} + \frac{1}{T_2^*}, \tag{1}$$

where T_2^* is the pure dephasing time.

In this paper we present the first demonstration of an electrically driven single-photon source capable of emitting indistinguishable photons. We first present results where the coherence time is measured as a function of current injection allowing us to choose the optimum operating conditions for our device. We then discuss two-photon interference experiments where the source is driven with a fixed[15] and pulsed voltage.[16]

2. SINGLE-PHOTON-EMITTING DIODE

The sample considered here is a p-i-n diode[14,17] as illustrated in Figure 2. The intrinsic region consists of a λ cavity with a layer of low density InGaAs/GaAs quantum dots at its center. The cavity is sandwiched between distributed Bragg reflectors above and below with two and twelve GaAs/$Al_{0.98}Ga_{0.02}As$ repeat layers respectively. A 40×40 μm mesa was etched and an ohmic n-contact and top Al p-contact were patterned. Apertures of 2 μm diameter were etched in the Al to isolate single quantum dots. Due to the large modal volume and low Q factor of the cavity there are no measurable cavity QED effects, the sole purpose of the cavity is to enhance the collection efficiency. Continuous wave (CW) emission can be produced by using a source measure unit (SMU) to supply a fixed bias, or combined with a pulse generator, the bias can be regulated to give pulsed emission.

3. DEPHASING DUE TO ELECTRICAL INJECTION

The electroluminescence (EL) spectra observed from an aperture on the device is shown in Figure 3(a). We identify two lines A and B which show no polarization splitting and are therefore attributed to charged exciton

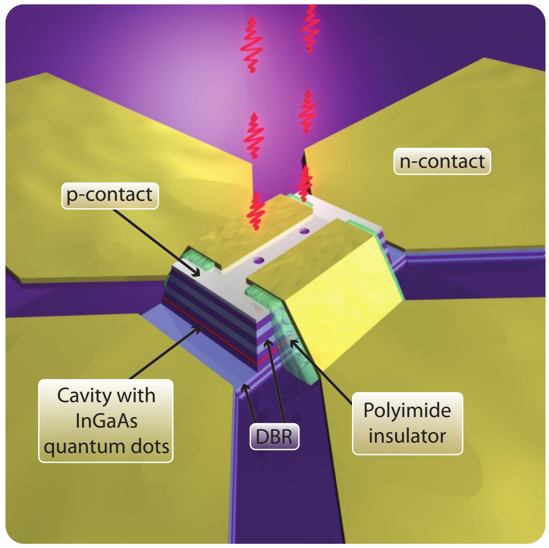

Figure 2. An illustration of our device. The p-i-n diode is formed by two distributed Bragg reflectors which are doped. The cavity, containing InGaAs/GaAs quantum dots, acts as the intrinsic region. Single quantum dots are isolated by etching apertures of 2 μm diameter in the Al top contact.

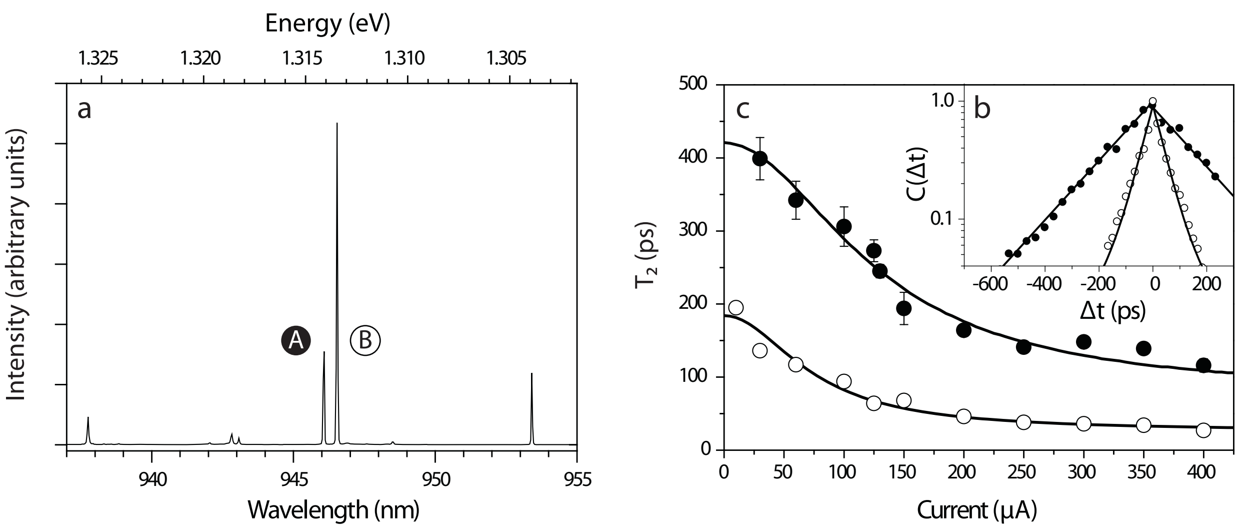

Figure 3. (a) Electroluminescence spectra from two charged excitons. Open circles correspond to dot A and solid circles to dot B. (b) Variation in fringe contrast as a function of the delay in the Michelson interferometer for a current of 200 μA. The shape of the plots are typical across the range of current studied. (c) Dependence of T_2 on current injection with theoretical fits.

states. We also note that adjusting the position of the collection optics alters the relative intensity of the two lines suggesting that they are from two spatially separate quantum dots.

Dephasing of the emitting state is measured by Fourier transform spectroscopy[9] and is carried out by inserting a Michelson interferometer in the emission path between the sample and detector. This technique allows accurate measurements of very narrow linewidths which are not possible with conventional diffraction grating spectrometers. Since dephasing causes homogenous broadening of the Lorentzian line shape, one would expect the fringe contrast $C(\Delta t) = \exp(-|\Delta t|/T_2)$ to decay at a faster rate as the temporal delay Δt in the interferometer is increased. Figure 3(b) shows a typical measurement of the fringe contrast as a function of Δt with a driving current of 200 μA. Dots A and B both show an exponential decay characteristic of a Lorentzian lineshape. In fact measurements at different driving current up to 400 μA all show a Lorentzian lineshape which suggests negligible inhomogeneous broadening. The variation in coherence time is shown in Figure 3(c). Both dots show a decrease in the coherence time with current. At a low current of 30 μA we measure a coherence time of 400 ps. This is a surprising result considering the incoherent nature of the excitation process. To explain the trend we fit the data according to the model by Berthelot et al.[11,18] As current flows through the device carriers may be trapped in impurities and defects in the wetting layer and then eventually escape. N traps in the vicinity of the dot will give rise to a fluctuating environment which induces a time varying Stark shift Δ of the exciton transition. The transition energy is randomized over a range given by the modulation amplitude

$$\Sigma = \frac{2\Sigma_s}{\sqrt{\frac{\tau_\uparrow}{\tau_\downarrow}} + \sqrt{\frac{\tau_\downarrow}{\tau_\uparrow}}}\,, \tag{2}$$

where $\Sigma_s = \sqrt{N}\Delta/2$ is the saturation value. The fluctuations occur on a timescale τ_f given by

$$\frac{1}{\tau_f} = \frac{1}{\tau_\uparrow} + \frac{1}{\tau_\downarrow}\,. \tag{3}$$

The carrier capture and escape rates $1/\tau_\downarrow$ and $1/\tau_\uparrow$, respectively, are

$$\frac{1}{\tau_\downarrow} = \frac{1}{\tau_2}(1 + n_2)\,, \tag{4}$$

$$\frac{1}{\tau_\uparrow} = \frac{1}{\tau_1}n_1 + \frac{1}{\tau_3}\left(\frac{I^\beta}{I^\beta + I_0^\beta}\right)\,, \tag{5}$$

where $n_i = 1/(\exp(E_i/k_BT) - 1)$ are the Bose-Einstein occupation factors. Subscripts 1 (2) pertain to acoustic (optical) phonon emission or absorption which can lead to carrier capture or escape respectively. τ_3 is the characteristic timescale for Auger emission and I_0 is the current at which the process saturates. The fitted curves in Figure 3(c) show the variation in coherence time $T_2 = \hbar^2/\Sigma^2\tau_f$. For the most part, since the material system is the same, we use similar parameters as Favero et al.[18] such that $\tau_1 = 200$ ps, $\tau_2 = 5$ ps, $E_1 = 1$ meV, $E_2 = 30$ meV, and $\beta = 2$ but with the fitting parameters $\tau_3 = 750$ ps, $I_0 = 300$ μA, and $\Sigma_s = 188$ μeV for dot A and $\tau_3 = 550$ ps, $I_0 = 200$ μA, and $\Sigma_s = 285$ μeV for dot B. This is reasonable since every quantum dot experiences a different charge environment. At high pump rates a transition from a Lorentzian lineshape to a Gaussian line is expected to occur when $\Sigma\tau_f/\hbar \geq 1$.[11] With a current of 200 μA, which is sufficient to saturate the quantum dot, we calculate this ratio to be 0.01 and 0.03 for dots A and B respectively further confirming that the lineshape is Lorentzian with negligible inhomogeneous broadening.

4. TWO-PHOTON INTERFERENCE

Measurements of the two-photon interference visibility were made using the Mach-Zehnder setup shown in Figure 4. The sample was driven with a fixed or pulsed bias at 4K. A polarizing beamsplitter (PBS) is used to select horizontally polarized photons which were then filtered using a spectrometer with a resolution of 88 μeV (not shown). By rotating a half-wave plate (HWP_1) the polarization of the emission can be aligned to the birefringence axis of the polarization-maintaining single-mode fiber. Emission is coupled into the fiber and split at the first fiber coupler C_1. It is then sent along two arms, one with a delay $\Delta\tau$, and the other with a second half-wave plate HWP_2. This waveplate can be adjusted to make the paths distinguishable or indistinguishable. A photon taking the long path is then able to interfere with a second photon emitted a time $\Delta\tau$ later and taking the short path at second fiber coupler C_2. This leads to a suppression in coincident counts at the two Si avalanche photodiode detectors D_1 and D_2. $\Delta\tau$ is chosen to be much greater than the coherence length of the photons so that only fourth-order interference occurs at C_2. Single-mode fiber allows the spatial modes to be easily matched at the final coupler.

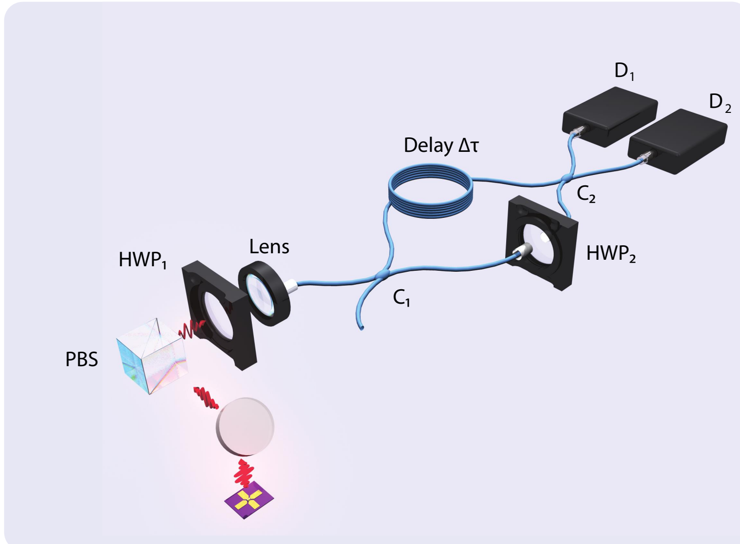

Figure 4. A simplified schematic of the setup. The diode is driven using a SMU for CW emission or combined with a pulse generator for pulsed emission. Two-photon interference is carried out using a fiber-coupled Mach-Zehnder interferometer. A polarizing beamsplitter (PBS) allows horizontally polarized photons selected. Half-wave plate (HWP_1) aligns the polarization to the axis of the polarization-maintaining single-mode fiber. A spectrometer (omitted for clarity) located between HWP_1 and the lens is used to filter the emission. The emission is then coupled into the fiber and split at the first coupler C_1. The two arms can be made distinguishable or indistinguishable by rotating HWP_2. For indistinguishable photons interference occurs at the final coupler C_2 resulting in a suppression of coincident counts at the two Si avalanche photodiode detectors D_1 and D_2.

4.1 Fixed bias operation

Here we describe CW two-photon interference measurements with the device operating at a fixed bias. Measurements were taken using dot A as the long coherence time would allow us to partially resolve the interference. The device was driven with a current of 100 μA at which point the intensity was at half the saturated value. This corresponds to a coherence time of ~ 325 ps and a Lorentzian linewidth of 4 μeV.

For a single photon emitted at a time t_0 and undergoing pure dephasing described by $\phi(t)$, the wavefunction has the form

$$|\psi\rangle \;\propto \int_{t_0}^{\infty} e^{-(t-t_0)/T_1 + i\phi(t)}\hat{\mathbf{e}}\, e^{-i(\mathbf{k}\cdot\mathbf{r}-\omega t)} a^\dagger |0\rangle\, dt\,. \tag{6}$$

It can be shown that for photons arriving in the same spatial mode $|\langle\psi_1|\psi_2\rangle|^2 = \cos^2(\theta)e^{-2|\tau|/T_2}$ where τ is the delay between detecting the photons. The form of this expression is derived from the fact that the quantum dot emits photons with a Lorentzian energy spectrum. For a dot emitting well below saturation, the pertinent equations describing our experiment are

$$g^{(2)}(\tau) = F_r(\tau) \otimes \left(1 - e^{-|\tau|/T_1}\right)\,, \tag{7}$$

$$\begin{aligned} g^{(2)}_{HOM}(\tau,\theta) \;\; = \;\; & F_r(\tau) \otimes \Big\{ 4\left(T_1^2 + R_1^2\right) R_2 T_2 g^{(2)}(\tau) \\ & + 4R_1T_1 \left(T_2^2 g^{(2)}(\tau - \Delta\tau) + R_2^2 g^{(2)}(\tau + \Delta\tau)\right)\left(1 - \cos^2(\theta)e^{-2|\tau|/T_2}\right)\Big\}\,, \end{aligned} \tag{8}$$

where $g^{(2)}(\tau)$ is the correlation measured using a Hanbury-Brown Twiss (HBT) interferometer[19] and $F_r(\tau)$ is the impulse response function (IRF) of our detection system. In Equation 8, R and T are the reflection and transmission intensity coefficients and θ is the difference in polarization between the two photons. The IRF was

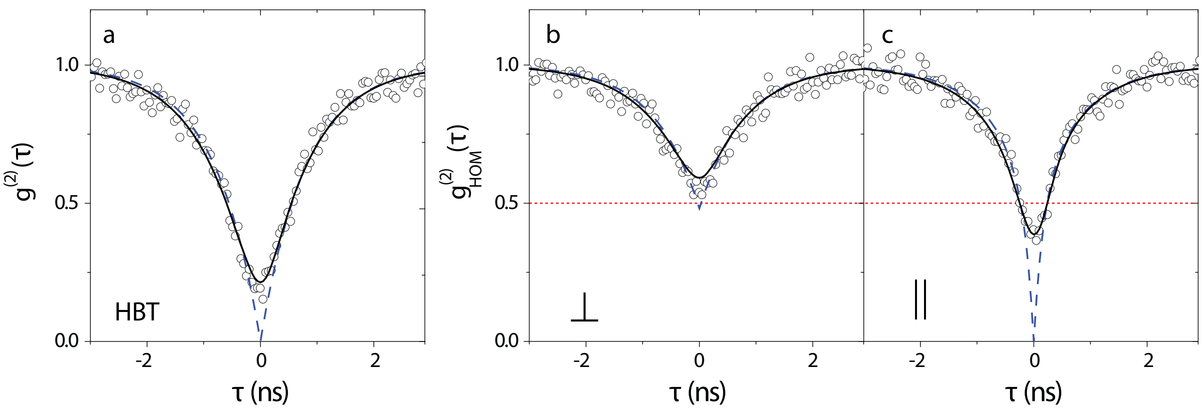

Figure 5. Hanbury-Brown and Twiss and two-photon interference results. In (a) to (c) dashed lines show ideal curves with perfect system response and solid lines model the effect of finite system response. The data is fitted with $T_1 = 800$ ps and $T_2 = 325$ ps. (a) Hanbury-Brown Twiss correlation, $g^{(2)}(\tau)$. (b) $g^{(2)}_{\perp}(\tau) = g^{(2)}_{HOM}(\tau, \theta = \pi/2)$, dotted line indicates the classical limit. (c) $g^{(2)}_{\parallel}(\tau) = g^{(2)}_{HOM}(\tau, \theta = 0)$.

measured by performing a HBT measurement using a mode-locked Ti-Sapphire laser tuned to 940 nm and can be approximated by a Gaussian function of FWHM, $\Gamma = 428\, ps$. A HBT measurement was taken to determine $g^{(2)}(\tau)$ of the source (Figure 5(a)). By plotting Equation 7 (solid line) and assuming a perfect single photon source with $T_1 = 800$ ps, we obtain a good fit to the data. We also plot $g^{(2)}(\tau)$ for a perfect system response (dashed line).

In Figures 5(b) and (c) we present detailed plots of the correlations around $\tau = 0$ ns for photons with mutually orthogonal and parallel polarizations, respectively. The data is fitted with $g^{(2)}_{\parallel}(\tau) = g^{(2)}_{HOM}(\tau, \theta = 0)$ and $g^{(2)}_{\perp}(\tau) = g^{(2)}_{HOM}(\tau, \theta = \pi/2)$ and $T_2 = 325$ ps, also shown for comparison are curves for a perfect system response (dashed lines). For photons with parallel polarization, we observe a dip at $\tau = 0$ ns below the limit where classical correlations occur, i.e. where coincident detections occur 50% of the time, as indicated by the dotted line. For orthogonally polarized photons the dip no longer goes below 50%. We also observe two dips to 75% at $\tau = \pm 10$ ns, due to the delay in the interferometer. Equality of these two dips suggests that $R_2 = T_2 = 0.5$. In the absence of any fitting parameters, our fits are in strong agreement with the measured data. To quantify the effect we observe, we define the two-photon interference visibility as $V_{\mathrm{HOM}}(\tau) = \left(g^{(2)}_{\perp}(\tau) - g^{(2)}_{\parallel}(\tau)\right)/g^{(2)}_{\perp}(\tau)$. We measure a visibility of 0.33 ± 0.06, consistent with the assumption that interference is entirely limited by the resolution of the detection system and that there is perfect overlap of the photon wavefunctions at C_2.

Finally, we consider ways in which we may post-select a higher visibility. Using Equation 8 and a Gaussian system response, we are able to estimate the visibility of interference (Figure 6) as a function of coherence time ($\Gamma = 428$ ps) or system resolution ($T_2 = 325$ ps). For the correlations we have performed, a narrow IRF and long coherence time are favorable such that the ratio $2\Gamma/T_2$ is minimized. From the fitted data in Figure 3(b) we expect the coherence time to reach a saturated value of ~ 420 ps at very low pump currents which corresponds to a visibility of ∼45%. It is clear that there is a far greater advantage to be had in improving the timing resolution. For example, if $\Gamma \sim 100$ ps one should be able to measure a visibility greater than 70%. This could be achieved using superconducting single-photon detectors,[20] for example.

4.2 Pulsed bias operation

In this section we report a new technique in obtaining indistinguishable photons from a triggered quantum dot single-photon source. We now turn our focus over to dot B which is the brighter of the two dots. In Figure 7(a) we show a voltage trace where the device is operated in the conventional way by applying a bias below threshold

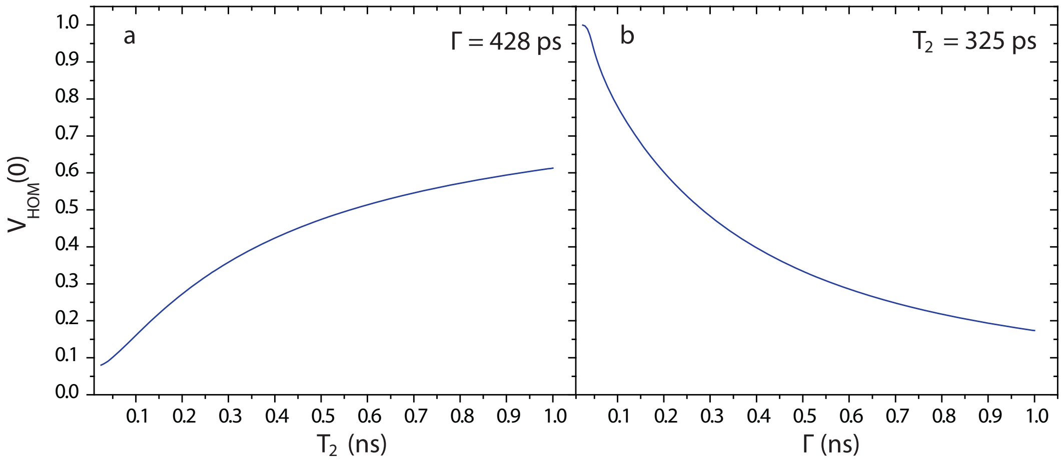

Figure 6. Numerical simulation showing the variation in V_{HOM} with (a) system resolution Γ ($T_2 = 325$ ps) and (b) coherence time T_2 ($\Gamma = 428\ ps$). A larger gain in visibility can be achieved by improving the detection resolution of the system.

and applying a series of pulses (nominally 300 ps long) to inject carriers into the device. The change in electric field causes the line to Stark shift into a spectral window where the emission is collected (Figure 7(b)). Here, carrier injection and collection of the emission occurs at the same time. This led to a multiphoton emission probability of $g^{(2)}(\tau) = 0.25 \pm 0.03$ (Figure 7(c)).

Optimum performance is achieved by superimposing a two-pulse sequence on a DC bias of $\sim$1.45 V (Figure 7(d)). To begin each cycle a positive-amplitude, 300 ps long, pulse injects carriers into the quantum dot. Immediately following, a second negative-amplitude pulse Stark shifts the emission line by 0.15 nm (200 μeV) into a spectral window where the photon is collected (Figure 7(e)). In contrast to the single-pulse method, injection and collection are separated in time. The temporal jitter can be reduced by applying a narrower negative-amplitude pulse, but with a reduction in count rate. This particular scheme serves two main purposes. As we saw in Section 3, current flowing through the device results in a shorter coherence time. With our technique the photon is collected when the diode is biased below threshold. Secondly, by carefully choosing the pulse amplitudes we are able to eliminate refilling of the dot. The negative-amplitude pulse also depopulates other emitting states which may contribute to multi-photon emission. As before, we perform a HBT measurement to test the quality of the single-photon source. From the data in Figure 7(f) we find that $g^{(2)}(\tau) = 0.03 \pm 0.01$ which is a vast improvement on the single-pulse scheme and is on par with quantum dot sources under quasiresonant excitation.[7]

Using the same interferometer arrangement as before and the two-pulse scheme, two-photon interference experiments were carried out driving the source with a repetition period of $\delta\tau_0 = 1.98$ ns. However, this time the delay in the interferometer was set to $\Delta\tau = \delta\tau_0$. By tuning the source repetition rate we are able to produce the characteristic HOM "dip" (Figure 8). The minimum is reached when $\Delta\tau = \delta\tau_0$. The raw two-photon interference visibility is $60 \pm 4\%$, while subtracting the dark counts the visibility increases to $64 \pm 4\%$. For spatially mode-matched photons this value is equal to the wave-function overlap $|\langle\psi_1|\psi_2\rangle|^2$.[21] Since this visibility is greater than $2g^{(2)}(0)$ it should be possible to generate polarization entangled photons[21] from this source. The dip is fitted using the theory by Legero et al.[22] In their original model the photons are described as a superposition of single-frequency modes and a Gaussian energy spectrum. We follow the same approach but for photons with a Lorentzian energy spectrum. We also incorporate a Gaussian jitter in the photon emission time and the effect of a time-varying Stark shift of the emitter. However, only the jitter in the emission time has a significant effect on the shape and depth of the dip. We obtain a very good fit if we assume that the jitter occurs within 31 ps. We also assume that $T_2 = 60$ ps, which was confirmed by an independent measurement. For $T_1 = 800$ ps we estimate $T_2^* = 62$ ps. Finally if a we consider pulsed optical excitation with the source held at a fixed bias we

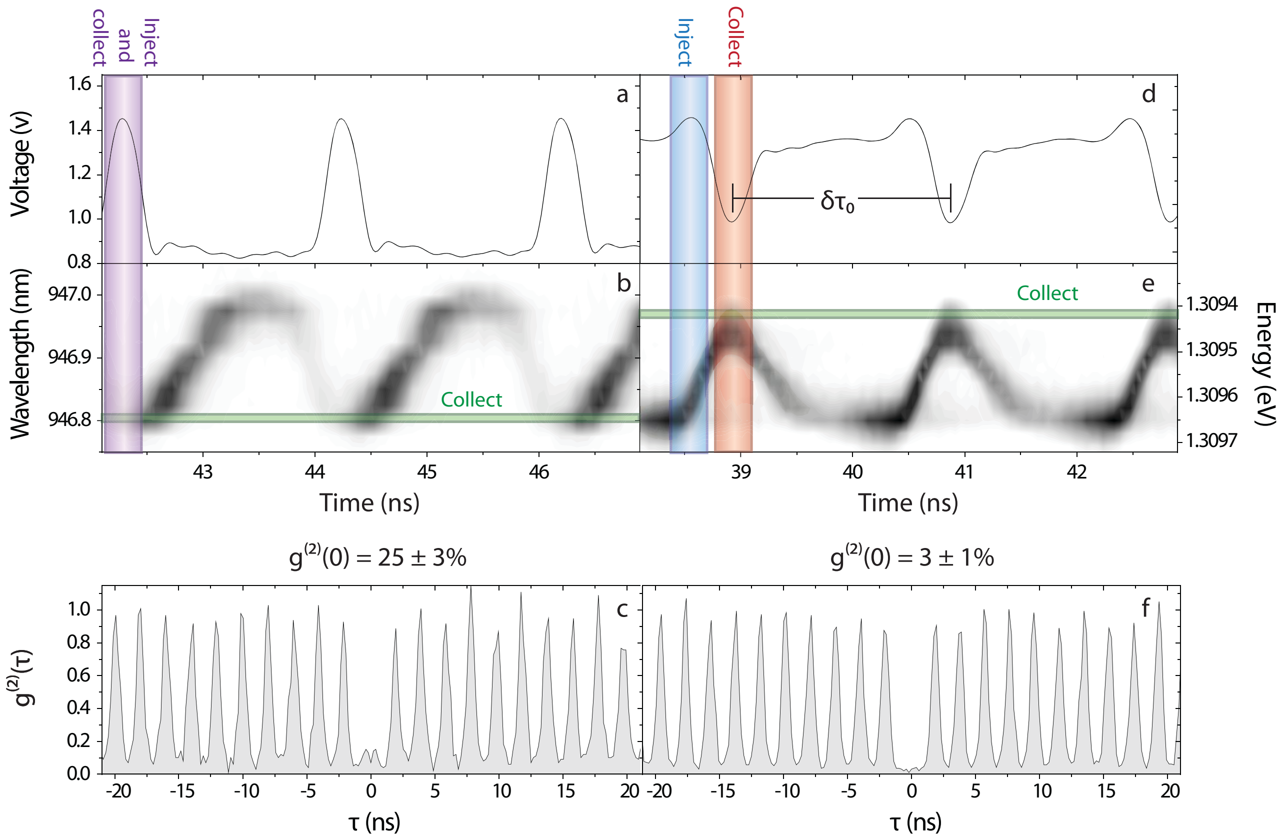

Figure 7. (a) Voltage trace when operating the device with a single pulse. The device is biased below threshold and a pulse is applied to inject carriers. (b) Contour plot showing the time-varying Stark shift of the emission. Injection and collection occur at the same time. (c) HBT correlation, $g^{(2)}(\tau) = 0.25 \pm 0.03$. (d)-(e) two-pulse operation of the diode. (d) The positive-amplitude pulse injects carriers into the quantum dot, and a negative amplitude pulse is applied 300 ps later. The sequence is applied with a period $\delta\tau_0$. (e) Time-varying Stark shift of the emission, injection and collection are temporally separated. (f) HBT correlation, $g^{(2)}(\tau) = 0.03 \pm 0.01$.

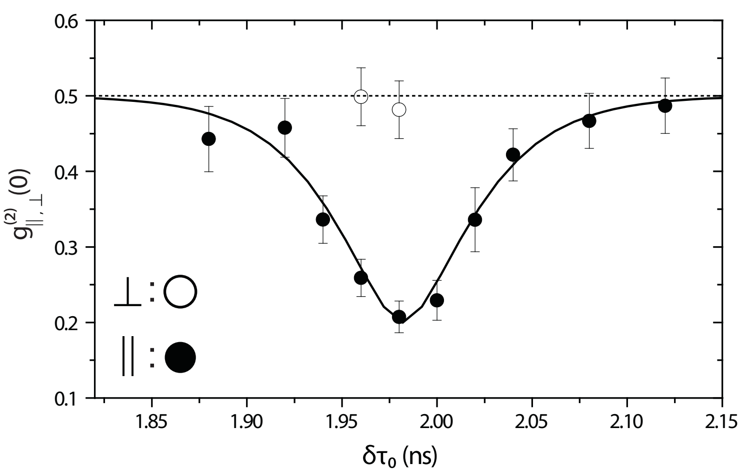

Figure 8. HOM-"dip" with 60% visibility. 0.5 is the classical limit.

can estimate the visibility as $T_2/2T_1 = 4\%$.[23] With this new technique we are able to achieve a much higher visibility without cavity QED effects.

5. CONCLUSION

In this paper we have demonstrated the first electrically driven single-photon source capable of emitting indistinguishable photons. Such a source is a step towards for compact, fast, and relatively cheap devices for scalable quantum information processing. We hypothesize that the low impurity and defect density of our sample gave rise to long coherence times up to 400 ps at low pump current, despite the incoherent nature of our scheme. By operating the device at a fixed bias a two-photon interference experiment was carried out without synchronizing the arrival of photons at a beamsplitter. The post-selected visibility in this case was limited only by the response of our detection system. By improving the detection system it should be possible to post-select a visibility above 70%. Alternatively, using a two-pulse scheme to select photons from a narrow time range it is possible to generate triggered single photons that have been emitted before dephasing takes place. The visibility of interference, from measurements of the HOM-"dip", is $64 \pm 4\%$ after dark count subtraction. The visibility may be improved by using a shorter negative-amplitude pulse or a source with a longer coherence time. With these improvements this source may be suitable for applications such as tests against local realism[24] and entanglement swapping.[25]

ACKNOWLEDGMENTS

This work was partially funded by the EU-projects QAP and SANDiE. One of the authors (R. B. P.) would also like to thank EPSRC and TREL for funding.

REFERENCES

[1] Hong, C. K., Ou, Z. Y., and Mandel, L., "Measurement of subpicosecond time intervals between two photons by interference," *Phys. Rev. Lett.* **59**, 2044 (1987).

[2] Shih, Y. H. and Alley, C. O., "New type of Einstein-Podolsky-Rosen-Bohm experiment using pairs of light quanta produced by optical parametric down conversion," *Phys. Rev. Lett.* **61**(26), 2921 (1988).

[3] Knill, E., Laflamme, R., and Milburn, G. J., "A scheme for efficient quantum computation with linear optics," *Nature (London)* **409**, 46 (2001).

[4] Kiraz, A., Ehrl, M., Hellerer, T., Müstecaplioğlu, O. E., Bräuchle, C., and Zumbusch, A., "Indistinguishable photons from a single molecule," *Phys. Rev. Lett.* **94**, 223602 (2005).

[5] Beugnon, J., Jones, M. P. A., Dingjan, J., Darquié, B., Messin, G., Browaeys, A., and Grangier, P., "Quantum interference between two single photons emitted by independently trapped atoms," *Nature (London)* **440**, 779 (2006).

[6] Maunz, P., Moehring, D. L., Olmschenk, S., Younge, K. C., Matsukevich, D. N., and Monroe, C., "Quantum interference of photon pairs from two remote trapped atomic ions," *Nature Phys.* **3**, 538 (2007).

[7] Santori, C., Fattal, D., Vučković, J., Solomon, G. S., and Yamamoto, Y., "Indistinguishable photons from a single-photon device," *Nature (London)* **419**, 594 (2002).

[8] Borri, P., Langbein, W., Schneider, S., Woggon, U., Sellin, R. L., Ouyang, D., and Bimberg, D., "Ultralong dephasing time in InGaAs quantum dots," (2001).

[9] Kammerer, C., Cassabois, G., Voisin, C., Perrin, M., Delalande, C., Roussignol, P., and Gérard, J. M., "Interferometric correlation spectroscopy in single quantum dots," *Appl. Phys. Lett.* **81**, 2737 (2001).

[10] Bayer, M. and Forchel, A., "Temperature dependence of the exciton homogeneous linewidth in $In_{0.60}Ga_{0.40}As/GaAs$ self-assembled quantum dots," *Phys. Rev. B* **65**, 041308(R) (2002).

[11] Berthelot, A., Favero, I., Cassabois, G., Voisin, C., Delalande, C., Roussignol, P., Ferreira, R., and Gérard, J. M., "Unconventional motional narrowing in the optical spectrum of a semiconductor quantum dot," *Nature Phys.* **2**, 759 (2006).

[12] Uskov, A. V., Magnusdottir, I., Tromborg, B., Mørk, J., and Lang, R., "Line broadening caused by coulomb carrier–carrier correlations and dynamics of carrier capture and emission in quantum dots," *Appl. Phys. Lett.* **79**, 1679 (2001).

[13] Gotoh, H., Kamada, H., Saitoh, T., Ando, H., and Temmyo, J., "Effects of biexcitons on exciton decoherence processes in $In_xGa_{1-x}As$ quantum dots," *Phys. Rev. B* **69**, 155328 (2004).

[14] Yuan, Z., Kardynal, B. E., Stevenson, R. M., Shields, A. J., Lobo, C. J., Cooper, K., Beattie, N. S., Ritchie, D. A., and Pepper, M., "Electrically driven single-photon source," *Science* **295**, 102 (2002).

[15] Patel, R. B., Bennett, A. J., Cooper, K., Atkinson, P., Nicoll, C. A., Ritchie, D. A., and Shields, A. J., "Post-selective two-photon interference from a continuous nonclassical stream of photons emitted by a quantum dot," *Phys. Rev. Lett.* **100**(20), 207405 (2008).

[16] Bennett, A. J., Patel, R. B., Shields, A. J., Cooper, K., Atkinson, P., Nicoll, C. A., and Ritchie, D. A., "Indistinguishable photons from a diode," *Appl. Phys. Lett.* **92**(19), 193503 (2008).

[17] Bennett, A. J., Unitt, D. C., See, P., Shields, A. J., Atkinson, P., Cooper, K., and Ritchie, D. A., "Microcavity single-photon-emitting diode," *Appl. Phys. Lett.* **86**, 181102 (2005).

[18] Favero, I., Berthelot, A., Cassabois, G., Voisin, C., Delalande, C., Roussignol, P., Ferreira, R., and Gérard, J. M., "Temperature dependence of the zero-phonon linewidth in quantum dots: An effect of the fluctuating environment," *Phys. Rev. B* **75**, 073308 (2007).

[19] Hanbury-Brown, R. and Twiss, R. Q., "Correlation between photons in two coherent beams of light," *Nature* **177**, 27–29 (1956).

[20] Gol'tsman, G. N., Korneev, A., Rubtsova, I., Milostnaya, I., Chulkova, G., Minaeva, O., Smirnov, K., Voronov, B., Słysz, W., Pearlman, A., Verevkin, A., and Sobolewski, R., "Ultrafast superconducting single-photon detectors for near-infrared-wavelength quantum communications," *Phys. Status Solidi C* **2**, 1480–1488 (2005).

[21] Fattal, D., Inoue, K., Vučković, J., Santori, C., Solomon, G. S., and Yamamoto, Y., "Entanglement formation and violation of Bell's inequality with a semiconductor single photon source," *Phys. Rev. Lett.* **92**(3), 037903 (2004).

[22] Legero, T., Wilk, T., Hennrich, M., Rempe, G., and Kuhn, A., "Quantum beat of two single photons," *Phys. Rev. Lett.* **93**(7), 070503 (2004).

[23] Santori, C., Fattal, D., Vuckovic, J., Solomon, G. S., and Yamamoto, Y., "Single-photon generation with InAs quantum dots," *New J. Phys.* **6**, 89 (2004).

[24] Aspect, A., Dalibard, J., and Roger, G., "Experimental test of Bell's inequalities using time-varying analyzers," *Phys. Rev. Lett.* **49**, 1804–1807 (1982).

[25] Halder, M., Beveratos, A., Gisin, N., Scarani, V., Simon, C., and Zbinden, H., "Entangling independent photons by time measurement," *Nature Phys.* **3**, 692 (2007).